X-644-70-319

PREPRINT

NASA TM X-65320

ELECTRON PARAMAGNETIC RESONANCE OF V^{2+}, Mn^{2+}, Fe^{3+} AND OPTICAL SPECTRA OF V^{3+} IN ZOISITE $Ca_2 Al_3 Si_3 O_{12} (OH)$

TUNG TSANG

SUBRATA GHOSE

AUGUST 1970

GSFC

GODDARD SPACE FLIGHT CENTER

GREENBELT, MARYLAND

X-644-70-319

ELECTRON PARAMAGNETIC RESONANCE OF V^{2+}, Mn^{2+}, Fe^{3+} AND OPTICAL SPECTRA OF V^{3+} IN ZOISITE $Ca_2 Al_3 Si_3 O_{12} (OH)$

Tung Tsang*

Subrata Ghose

Planetology Branch

August 1970

GODDARD SPACE FLIGHT CENTER

Greenbelt, Maryland

*Permanent address: Department of Physics, Howard University, Washington, D. C. 20001.

ELECTRON PARAMAGNETIC RESONANCE OF V^{2+}, Mn^{2+}, Fe^{3+} AND OPTICAL SPECTRA OF V^{3+} IN ZOISITE $Ca_2\ Al_3\ Si_3\ O_{12}\ (OH)$

Tung Tsang

Subrata Ghose

Planetology Branch

ABSTRACT

Electron paramagnetic resonance and optical absorption spectra have been used to clarify the local environments of transition metal ions and their distributions among various Al- and Ca-sites in a gem quality zoisite crystal from Tanzania. The EPR spectra due to Mn^{2+}, Fe^{3+} and two types of V^{2+} have been interpreted by the spin Hamiltonian

$$\beta \mathbf{H} \cdot \mathbf{g} \cdot \mathbf{S} + \mathbf{I} \cdot \mathbf{A} \cdot \mathbf{S} + D\left[S_z^2 - \frac{1}{3} S(S+1)\right] + E\left(S_x^2 - S_y^2\right)$$

in the principal axes system x, y, z. The Mn^{2+} ions occupy one of the Ca-sites, probably Ca(1), with point group symmetry m; g = 2.003 ± 0.005 and $|A|$ = (85 ± 2) $\times 10^{-4}$ cm^{-1}, both isotropic and also $|D|$ = (103 ± 5) $\times 10^{-4}$ cm^{-1}, $|E|$ = (34 ± 2) $\times 10^{-4}$ cm^{-1}, in general agreement with other oxides and hydrates. Highly anisotropic hyperfine and small zero-field splittings ($|D| < 0.014$ cm^{-1}) are observed for V^{2+}, which is the opposite of the usual situation. One of the two types of V^{2+} apparently occupies the same site as Mn^{2+}; the other V^{2+} ion is in a general position, and probably occupies a double minima potential around the Ca(2)

site. The Fe^{3+} ions occupy the Al_{II} site, since the point group symmetry is m; the principal axes, however, are displaced approximately 45° from the NMR axes of ^{27}Al. Apparently, the local environment changes when Al^{3+} ions are replaced by Fe^{3+}. For Fe^{3+}, we found $|D| = 0.14 \pm 0.03\ cm^{-1}$ and $|E| \sim 0.1\,|D|$. The optical absorption of V^{3+} and the trichroism of the zoisite single crystal are consistent with the two types of Al^{3+} site symmetries, with crystal field parameters Dq = 1850 and 1400 cm^{-1} at Al_I and Al_{II} sites.

CONTENTS

ELECTRON PARAMAGNETIC RESONANCE OF V^{2+}, Mn^{2+}, Fe^{3+} AND OPTICAL SPECTRA OF V^{3+} IN ZOISITE $Ca_2 Al_3 Si_3 O_{12}$ (OH)

INTRODUCTION

The crystal structure of zoisite, the orthorhombic form of $Ca_2 Al_3 Si_3 O_{12}$ (OH), was first proposed by Ito[1] and was recently refined by Dollase.[2] The aluminum-oxygen octahedra in zoisite are the most distorted among all known alumino-silicate structures. Brinkmann, Staehli and Ghose[3] studied the local environment of Al^{3+} by nuclear magnetic resonance (NMR) and confirmed this distortion by their large ^{27}Al quadrupole coupling constants.

Gem quality single crystals of zoisite from Tanzania are trichroic[4] (**E** ∥ **a**, green; **E** ∥ **b**, blue; **E** ∥ **c**, red-violet). In view of the strong local distortions from octahedral symmetry and also because of the interesting optical properties, we will present the results of paramagnetic resonance and optical studies on such a gem quality zoisite crystal in this paper, where the nearest neighbor environments have been studied via the transition metal ions and their *d*-orbitals. Furthermore, the distribution of transition metal ions among various calcium and aluminum sites in the zoisite crystal is an interesting but little understood problem, which may be studied also through the electron paramagnetic resonance experiments.

Zoisite is orthorhombic, space group P*nma*, with $a_0 = 16.212 \pm 0.008$ Å, $b_0 = 5.559 \pm 0.006$ Å, $c_0 = 10.036 \pm 0.004$ Å. The structure consists of endless

octahedral chains running parallel to the b-axis, which are formed of two types of Al-O octahedra sharing edges. These chains are cross-linked by isolated tetrahedral SiO_4 and Si_2O_7 groups and two types of CaO_7 polyhedra. From the structural refinement of Dollase,[2] an idealized view of the complex octahedral chains and a partial projection of the structure on (010)-plane has been given by Brinkmann, Staehli and Ghose;[3] their notation[3] for the Al-sites will be followed here; our Al_I and Al_{II} are Dollase's[2] Al(1, 2) and Al(3) respectively. The aluminum atoms occur in two crystallographically different positions. The first, Al_I, is in an eightfold general position 8(*d*) with point group symmetry 1, while the second, Al_{II}, is in a fourfold special 4(*c*) position with point group symmetry *m*.

Following Dollase,[2] the two calcium sites in zoisite will be denoted as Ca(1) and Ca(2) respectively. Both occur in special position 4(*c*) with point group symmetry *m*, the mirror plane being the (010)-plane. A view of the structure of zoisite is shown in Figure 1.

EXPERIMENTAL

The crystal axes and faces of the zoisite crystal were identified through the morphological studies of Hurlbut.[4] Chemical analysis[4] indicates the presence of approximately 0.13% V and 0.03% Fe by weight, and also the presence of trace quantities of Mn and Cr in the 10-100 ppm range.

A Varian type E-9 EPR spectrometer has been used for our measurements. The magnetic field scan was calibrated by the proton magnetic resonance frequency, and the microwave frequency was derived from observing a free radical

resonance signal. The spectra have been observed at room temperature near 9.3 GHz with the magnetic field **H** at various angles in the (100), (010) and (001) planes. Three examples are shown in Figure 2. Numerous resonance lines have been observed; sometimes, the weaker lines were obscured and could not be identified. For **H** parallel to the crystallographic **a**-axis (top trace of Figure 2), four different sets of resonance lines can be clearly identified, the single intense line on the left from Fe^{3+}, the intense six-line Mn^{2+} central ($-1/2 \rightarrow 1/2$) transitions with the weak inner satellite pair ($\pm 1/2 \rightarrow \pm 3/2$) marked by m′ and m″, and two inequivalent eight-line V^{2+} central transitions marked by V_1 and V_2. The Mn^{2+} satellites, marked by m′ and m″, may be identified from their hyperfine splitting, which is identical to that of the central transition.

Following the standard notations,[5,6] we will describe our experimental results by the spin Hamiltonian $\mathcal{H}$ in the principal coordinate system (x, y, z):

$$\mathcal{H} = \beta\left(g_z H_z S_z + g_x H_x S_x + g_y H_y S_y\right) + D\left[S_z^2 - \frac{1}{3} S(S+1)\right]$$

$$+ E\left(S_x^2 - S_y^2\right) + A_z S_z I_z + A_x S_x I_x + A_y S_y I_y \,. \qquad (1)$$

The magnitudes of the spin Hamiltonian parameters and the orientations of the principal axes can be correlated to the local environments and to the deviations from octahedral symmetry of the transition metal ions.

Mn^{2+} RESONANCE

For **H** in the (100) and (001) planes at various angles, sharp six-line patterns, similar to the top two traces of Figure 2, were always observed for the central $(-1/2 \rightarrow 1/2)$ transition of Mn^{2+}. For **H** in the (010) plane away from either the **a** or **c** axis, however, the six-line pattern quickly disappeared, an example being the bottom trace of Figure 2. We therefore conclude that the point group symmetry of Mn^{2+} site is m, the (010) plane being the mirror plane. Hence, for **H** in the (100 and (001) planes, the Mn^{2+} resonances are actually superpositions of two identical spectra related to each other through the mirror plane.

The hyperfine splittings appear to be independent of orientation of **H** within experimental uncertainties. Our experimental data give $|A| = (85 \pm 2) \times 10^{-4}\ cm^{-1}$. (Standard deviations will be used throughout this paper.)

Often, the inner satellite pairs ($\pm 1/2 \rightarrow \pm 3/2$ transitions) are clearly observable; they may be identified from the characteristic hyperfine splitting. The separations between central $(-1/2 \rightarrow 1/2)$ component and satellite $(\pm 1/2 \rightarrow \pm 3/2)$ are summarized in Figure 3(a) and (b) for **H** in the (010) and (001) planes. Since the **b**-axis is one of the principal directions, these data may be used to evaluate the spin Hamiltonian parameters D and E; the results are $|D| = (103 \pm 5) \times 10^{-4}$ cm^{-1}, $|E| = (34 \pm 2) \times 10^{-4}\ cm^{-1}$. The **x**-axis is along the crystallographic **b**-axis. Since within the experimental error, $D = 3E$, the choice between **y** and **z** is somewhat arbitrary; they are displaced by $5° \pm 1°$ from the **a** and **c** axis in the (010)-plane. Because $|D|$ and $|E|$ are small, perturbation theory may be

used for line positions. The calculated separations are also shown in Figure 2(a) and (b); they agree well with our data.

In Figure 3(c), we have compared the separations between the central transitions of the two different Mn^{2+} ions for **H** in the (010)-plane with second-order perturbation calculations. Again the agreement is reasonable.

We have calculated g from the positions of the central transitions after second order perturbation corrections.[5] We found $g = 2.003 \pm 0.005$ to be isotropic within experimental error.

The experimental values of g and A and the lack of angular dependence are in general agreement with other Mn^{2+} values[6] for oxides and hydrates. From the observed D and E, we conclude that the Mn^{2+} site symmetry is m, the (010)-plane being the mirror plane, and the distortion from octahedral symmetry is small. In the zoisite crystal, there are two inequivalent Ca^{2+} sites, (Figure 1) denoted as Ca(1) and Ca(2) by Dollase;[2] both sites have point group symmetry m, the (010)-plane being the mirror plane. It is likely that Mn^{2+} replaces Ca^{2+} in Ca(1)-positions, where the Ca-O distances are not very different from each other, and also the distortion is approximately along the **a**-axis. Furthermore, the average Ca(1)-O distance, 2.46 Å is smaller than the average Ca(2)-O distance, 2.55 Å and hence, the Ca(1)-site is more favorable for Mn^{2+}.

V^{2+} RESONANCE

Two types of V^{2+} central ($-1/2 \rightarrow 1/2$) transitions were observed, denoted as V_1 and V_2 respectively. This is illustrated by the top spectra of Figure 2.

For both resonances, the central transition field strength (obtained by averaging over the eight hyperfine components) varied only slightly (< 10 G) for different orientations of **H**. From our data, we found that the **g**-tensor is isotropic with $g = 1.940 \pm 0.007$ for both V_1 and V_2 resonances. Previous paramagnetic resonance studies[7] of V^{2+} in oxides, halides and hydrates have given isotropic g-values between 1.95 and 1.99, and are consistent with our zoisite results. From the maximum variation (approximately 10 G) of the central transition field strength, we also estimate that $|D| < 0.014\ cm^{-1}$ from second order perturbation calculations.[5,6] The $V_1 : V_2$ resonance intensity ratio is about 2:1, indicating a preference of V^{2+} for the V_1-site.

Surprisingly the hyperfine splittings of both types of V^{2+} resonances are highly anisotropic. For example, in the top and middle spectra of Figure 2, the V_2' hyperfine splitting changed from 126 to 157 G when the crystal was rotated by only 18°. So far, reports on V^{2+} resonances[7] in distorted octahedral environments have shown the opposite behavior, that is, large D ($\sim 0.1\ cm^{-1}$) but no anisotropy in the hyperfine splitting.

The angular variations of V_1 hyperfine splittings are summarized in Figure 4 for **H** in (100), (010) and (001)-planes. The spatial average of A is $(88 \pm 4) \times 10^{-4}\ cm^{-1}$, and is in general agreement with V^{2+} hyperfine splittings observed in oxides, halides and hydrates.[6,7] From Figure 4, the V_1 site symmetry may be readily identified as m, the mirror plane being the (010)-plane, since the rotation patterns with **H** in either the (100) or (001)-planes are symmetric, each

resonance line being the superposition of two symmetry-related lines. Thus the **b**-axis is one of the principal axes of the hyperfine tensor. From the rotation pattern with **H** in the (010)-plane (Figure 4b), we found that the other two principal axes differ from the crystallographic **a** and **c**-axes by 7 ± 2°. Within the experimental errors, the principal axes systems of V_i spin Hamiltonian are identical with the Mn^{2+} axes. Thus it appears that V^{2+} ions of type 1 occupy the same site as Mn^{2+}, i.e. the Ca(1) site.

Unfortunately, the V_2 resonance spectra are often obscured and only a partial analysis can be made. The results are summarized in Figure 5. The spatial average of A is $(100 \pm 6) \times 10^{-4}$ cm^{-1} and is not too different from the V_1 value. It is clear from Figure 5 that the (010)-plane is not a mirror plane at the V_2-site. Ionic radius and charge considerations restrict V^{2+} ions to one of the two Ca^{2+} sites, both of them however have site symmetry m with the (010)-plane as the mirror plane.[2] The geometry of the nearest neighbor oxygen atoms around the Ca(2) site is somewhat unfavorable to accommodate the V^{2+} ion; a plausible explanation of our resonance data is that the V^{2+} ion is situated in a double minima potential around the Ca(2) site and has shifted slightly away from the mirror plane.

Fe^{3+} RESONANCE

The intense resonance line in Figure 2 was identified as Fe^{3+} because of the lack of hyperfine splitting and because chemical analysis of our sample has shown the presence of considerable amount of Fe^{3+} (~0.03% by wt.). The Fe^{3+}

resonance line positions are summarized in Figure 6 for various magnetic field orientations. The line positions are highly anisotropic. We therefore expect the satellite lines to be quite weak and not readily observable.

For **H** in the (100)- and (001)-planes, single resonance lines are observed (see Figures 4a and 4c); thus the Fe^{3+} site must have point group symmetry *m*, the (010)-plane being the mirror plane. Also, from Figure 4b with **H** in the (010)-plane, it can be seen that the principal axes are displaced from the **a**- and **c**-axes by 44° ± 1°. Thus, for Fe^{3+} ions, the principal **x**-axis is along the direction of crystallographic **b**-axis, whereas the **y** and **z**-axes are in the (010)-plane, and are rotated by 44° ± 1° from the **a** and **c**-axes.

Charge and ionic radius considerations would place Fe^{3+} in one of the aluminum sites. Since Al_I is in a general position whereas Al_{II} has point group symmetry *m* with (010)-plane as the mirror plane, we conclude that the Fe^{3+} ions are located on the Al_{II} site. The directions of the principal axes, however, do not agree with the nuclear quadrupole resonance results.[3] Whereas the principal axes[3] of ^{27}Al at Al_{II} site are very close to the crystallographic axes, the Fe^{3+} principal axes are 44° away from **a** and **c**. Thus it appears that under certain conditions, the local environment changes when Al^{3+} ions are replaced by Fe^{3+}. A similar situation has been observed in spodumene, $LiAlSi_2O_6$. The principal axes for the Fe^{3+} spin Hamiltonian[8] was found to be quite different from the principal axes of the ^{27}Al quadrupole coupling tensors,[9] although both ions are located at sites with point group symmetry *m*.

For Fe^{3+} in zoisite, the rotation patterns for **H** perpendicular to the three principal axes are shown in Figure 6b and 6d. Clearly, the zero-field splitting has approximately cylindrical symmetry, (the experimental points shown as circles in Figure 6b and 6d have approximately the same angular variations, and the positions of the crosses in Figure 6d vary only slightly with the angle.) Therefore, $|E| << |D|$; in this case, the resonance condition for $\mathbf{H} \parallel \mathbf{z}$ is given by $g_z \beta \mathbf{H} = g_{\parallel} \beta \mathbf{H} = h\nu$ and is independent of the magnitude of $|D|$. From the observed resonance frequency (3390 G at 9.30 GHz), we found $g_z = 1.96 \pm 0.01$, in general agreement with previous studies[6] of Fe^{3+} in oxides and hydrates.

We have also estimated the zero field splittings of Fe^{3+} from our data. The spin Hamiltonian matrix for cylindrical symmetry ($E = 0$) was diagonalized, and the calculated values at various orientations of **H** were compared with data in Figure 6. We found $|D| = 0.14 \pm 0.03\ cm^{-1}$; the experimental uncertainty is fairly large, because satellite lines are weak and are not distinguishable from Mn^{2+} and V^{3+} resonance lines.

OPTICAL ABSORPTION OF V^{3+}

The polarized optical absorption spectra of zoisite in the visible range are summarized in Figure 7, with **E** parallel to the three principal crystallographic axes. The absorption bands are broad because of the large deviations from octahedral symmetry. The optical absorptions are due to electronic transitions between d-orbitals of V^{3+}, since the amounts of Cr and Mn are small, and the

extinction coefficients of Fe^{3+} are quite weak[10] in epidote, whose structure is similar to that of zoisite.

The ground state of V^{3+} is $^3T_1$, and the lowest energy absorption band of V^{3+} is the $^3T_1 \rightarrow {}^3T_2$ transition.[11] From the observed average wavelength 7700 Å, we obtain[12] $Dq = 1400\ cm^{-1}$ for the octahedral crystal field parameter. This is considerably smaller than $Dq = 1860\ cm^{-1}$ for[13] V^{3+} in Al_2O_3, where the average metal-oxygen distance is 1.91 Å. In zoisite, the average metal-oxygen distances[2,3] are 1.89 and 1.97 Å for Al_I and Al_{II} sites (point group symmetries 1 and m). Since crystal field parameter Dq varies approximately as the inverse fifth power of distance, the absorption band near 7700 Å is assigned to the type II sites. The Liehr-Ballhausen[12] calculated positions for the $^3A_2$, $^3T_1$ and $^1A_1$ bands are indicated by arrows in Figure 7 for $Dq = 1400\ cm^{-1}$. McClure[11] has shown for V^{3+}-Al_2O_3 that for the $^3T_2$ band, the absorption intensity vanishes when the polarized light **E**-vector lies in a plane of symmetry. This agrees with our zoisite data, the mirror plane being perpendicular to the **b**-axis, and the 7700 Å absorption peak for **E** ∥ **b** is considerably stronger than the peaks for either **E** ∥ **a** or **E** ∥ **c**. McClure[11] has also shown that, on the other hand, the intensity of the $^3T_1$ band is maximum for the **E**-vector along the direction of the axial distortion. The local environment of the type II site is a distorted oxygen octahedron compressed along the **a**-axis; the 4500 Å absorption peak ($^3T_1 \rightarrow {}^3T_1$) for **E** ∥ **a** is also considerably more intense than the **E** ∥ **b** and **E** ∥ **c** peaks.

Because of the absence of any point group symmetry at the Al_I-site, the anisotropy in absorption intensities is expected to be less pronounced. The crystal field parameter Dq for the type I site is probably not too different from the V^{3+}-Al_2O_3 value,[13] since the average metal-oxygen distances, 1.89 and 1.91 Å are almost identical. The calculated peak positions for $Dq = 1850\ cm^{-1}$ are shown as dashed arrows in Figure 6, and are in reasonable agreement with the observed spectra.

The absorption intensities for type I and II sites are not very different, indicating approximately random distributions of V^{3+} ions among the two types of sites. There are twice as many type I sites as type II in the zoisite crystal.[2,3]

DISCUSSION

The paramagnetic resonance, and optical absorption results have clarified the nature of the local environments of transition metal ions in zoisite; the spin Hamiltonian parameters and principal axes orientations have been listed in Table I. Our results may be summarized as follows.

(a) For the Mn^{2+} paramagnetic resonance, the zero field splittings $|D| = (103 \pm 5) \times 10^{-4}\ cm^{-1}$ and $|E| = (34 \pm 2) \times 10^{-4}\ cm^{-1}$ are relatively small; from the principal axes of the fine structure tensor, the point group symmetry was found to be m with (010)-plane as the mirror plane. The paramagnetic resonance data suggest that Mn^{2+} ions occupy one of the two Ca-sites,[2] probably Ca(1), in agreement with ionic radius and charge considerations. The observed isotropic $g = 2.003 \pm 0.005$

and $|A| = (85 \pm 2) \times 10^{-4}$ are in general agreement with previous observations on oxides, halides and hydrates.

(b) Two types of V^{2+} paramagnetic resonances have been observed. For both types, we found $g = 1.940 \pm 0.007$ to be isotropic within experimental error and also we found very small zero field splittings, $|D| < 0.014\ cm^{-1}$. Both hyperfine splittings are highly anisotropic. From the principal axes of the **A**-tensor, we conclude that one of the two types of V^{2+} ions occupies the same site as Mn^{2+} i.e., the Ca(1) site. The other one was found in a general position, and is probably located in a double-minima potential at the Ca(2) site.

(c) The highly anisotropic hyperfine splittings $|A|$ and the small zero-field splittings ($|D| < 0.014\ cm^{-1}$) for V^{2+} ions in zoisite are the opposite of previous results of V^{2+}-ions in distorted octahedral environments (isotropic $|A|$ and larger $|D| \sim 0.1\ cm^{-1}$). We have no explanation for this discrepancy at present.

(d) From the Fe^{3+} resonance data, the point group symmetry was found to be m with (010)-plane as the mirror plane, which places Fe^{3+} ions in the Al_{II} site.[2,3] The principal axes of Fe^{3+} spin Hamiltonian are approximately 44° away from the crystallographic axes, with $|D| = 0.14 \pm 0.03\ cm^{-1}$ and $|E| \sim 0.1\,|D|$. On the other hand, the principal axes of the ^{27}Al electric quadrupolar coupling tensor[3] at the Al_{II} site are very close to the crystallographic axes. Apparently, the local environment changes when Al^{3+} ions are replaced by Fe^{3+}.

(e) From the optical absorption spectra of V^{3+}, the crystal field parameter Dq was found to be 1850 cm^{-1} and 1400 cm^{-1} respectively, for V^{3+} in Al_I and Al_{II} sites. The trichroism of zoisite crystals has also been correlated to the point group symmetries of the aluminum sites.

ACKNOWLEDGMENT

We kindly thank Professor C. S. Hurlbut Jr. of Harvard University for the loan of the zoisite crystal, Professors H. Devoe and G. Atkinson of the University of Maryland for the use of the Cary 14 spectrophotometer and Mrs. E. H. Glover for computer programming.

REFERENCES

1. T. Ito, N. Morimoto and R. Sadanaga, Acta Cryst. 7, 53 (1954).

2. W. A. Dollase, Amer. Mineralogist 53, 1882 (1968).

3. D. Brinkmann, J. L. Staehli and S. Ghose, J. Chem. Phys. 51, 5128 (1969).

4. C. S. Hurlbut Jr., Amer. Mineralogist 54, 702 (1969).

5. See the review by W. Low, Paramagnetic Resonance in Solids (Academic Press, New York, 1960) Section 8.

6. See the review by S. A. Altshuler and B. M. Kozyrev, Electron Paramagnetic Resonance (Academic Press, New York, 1964).

7. I. Y. Chan, D. C. Doetschman, C. A. Hutchison Jr., B. E. Kohler and J. W. Stout, J. Chem. Phys. 42, 1048 (1965); references have also been given by these authors on previous paramagnetic resonance studies of V^{2+}.

8. A. Manoogian, F. Holuj and J. W. Carswell, Canadian J. Phys. 43, 2262 (1965).

9. H. E. Petch, N. G. Cranna and G. M. Volkoff, Canadian J. Phys. 31, 837 (1953).

10. R. G. Burns and R. G. J. Strens, Mineralogical Magazine 36, 204 (1967).

11. D. S. McClure, J. Chem. Phys. 36, 2757 (1962).

12. A. D. Liehr and C. J. Ballhausen, Ann. Phys. (New York) 6, 134 (1959).

13. D. S. McClure, Electronic Spectra of Molecules and Ions in Crystals (Academic Press, New York, 1959), p. 134.

Table 1

Spin-Hamiltonian Parameters in Zoisite

	Mn^{2+}	V_1^{2+}	V_2^{2+}	Fe^{3+}
g	2.003 ± 0.005 isotropic	1.940 ± 0.007 isotropic	1.940 ± 0.007 isotropic	$g_z = 1.96 \pm 0.01$
|D|	$(103 \pm 5) \times 10^{-4}$ cm^{-1}	< 0.014 cm^{-1}	< 0.014 cm^{-1}	0.14 ± 0.03 cm^{-1}
|E|	$(34 \pm 2) \times 10^{-4}$ cm^{-1}	< 0.005 cm^{-1}	< 0.005 cm^{-1}	$<<$ |D|
Average |A|	$(85 \pm 2) \times 10^{-4}$ cm^{-1} isotropic	$(88 \pm 4) \times 10^{-4}$ cm^{-1} anisotropic	$(100 \pm 6) \times 10^{-4}$ cm^{-1} anisotropic	none
Site symmetry	m	m	1	m
Mirror plane	(010)	(010)	none	(010)
Angle[a] between principal and crystallographic axes	5° ± 1°	7° ± 2°	---	44° ± 1°

[a]The two coordinate systems are related to each other by a rotation about the b-axis.

LIST OF FIGURES

Figure 5. Angular dependence of hyperfine splitting (Gauss) of V^{2+} resonance of type 2. (a) **H** in (100)-plane, angle from **c**-axis, (b) **H** in (001)-plane, angle from **a**-axis.

Figure 6. Angular dependence of Fe^{3+} central transition at 9.30 GHz. Top to bottom: (a) **H** in (100)-plane, angle from **b**-axis; (b) **H** in (010)-plane, angle from **a**-axis, (c) **H** in (001)-plane, angle from **a**-axis, (d) **H** in the plane that bisects the (100)- and (001)-planes, angle from **b**-axis.

Figure 7. Optical densities of V^{3+} vs. wavelength λ (in 10^{-4} cm) in zoisite; solid, dotted and dashed lines are for **E** $\parallel$ **a**, **b** and **c** respectively; the solid and dashed arrows are for peak positions calculated for type I and II sites (Dq = 1850 and 1400 cm^{-1}). Optical density is for 1 cm thick sample for $\lambda > 0.4$, and for 0.5 cm thick sample for $\lambda < 0.4$.

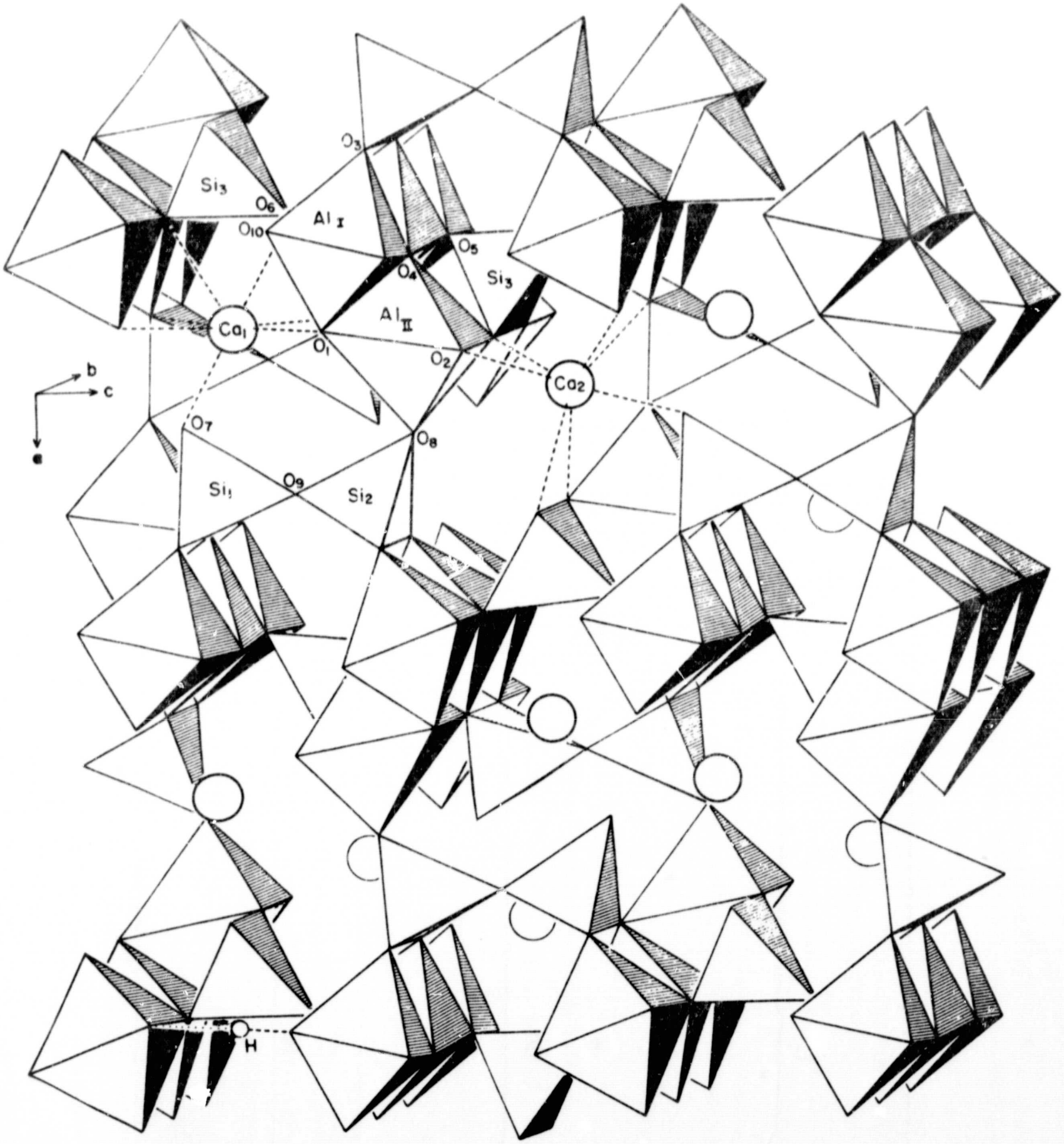
O3
Si3
O6
O10
Al I
O5
O4
Si3
Al II
Ca1
O1
O2
Ca2
b
c
a
O7
O8
Si1
O9
Si2
H

Fig. 1.

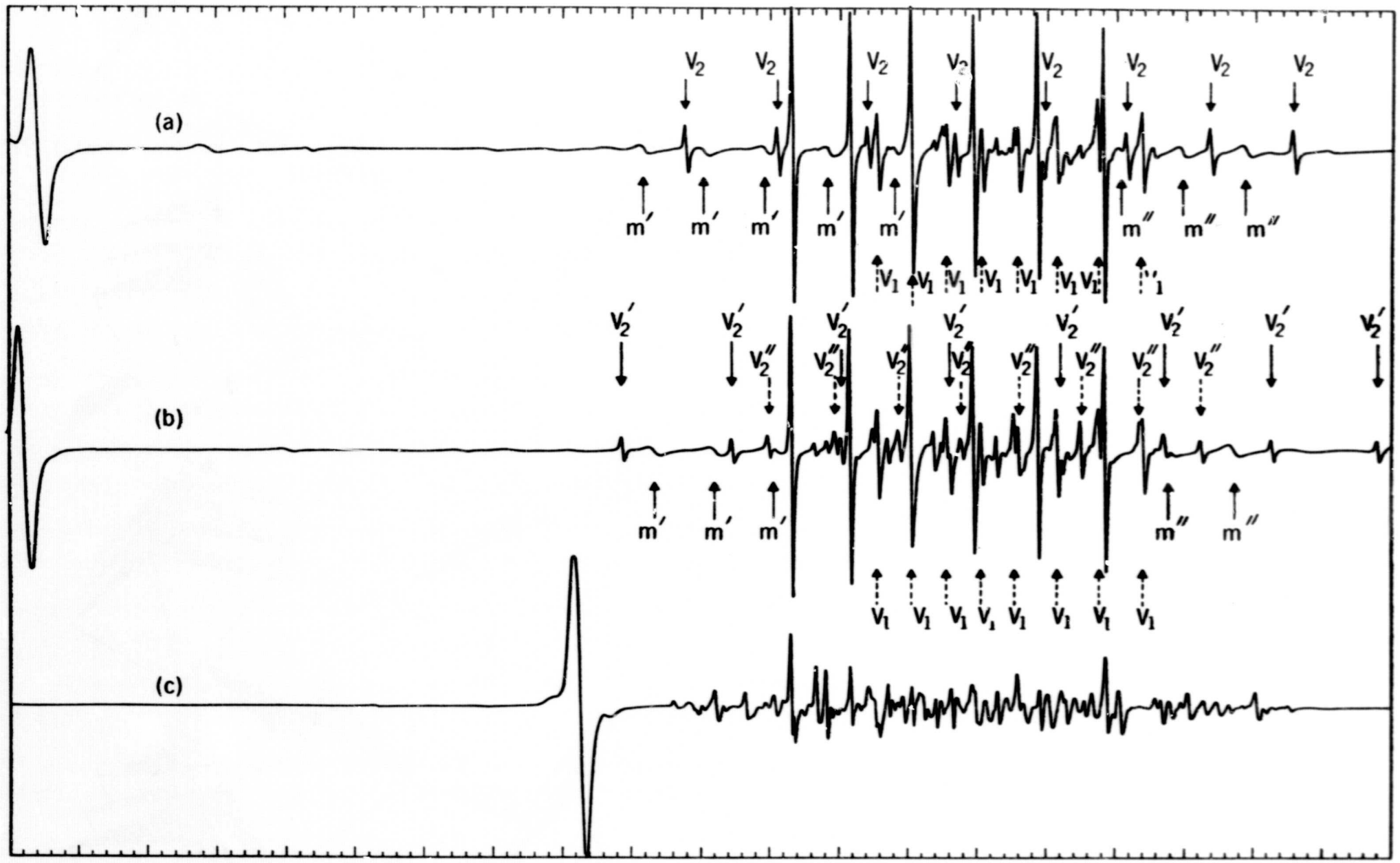

Fig. 2.

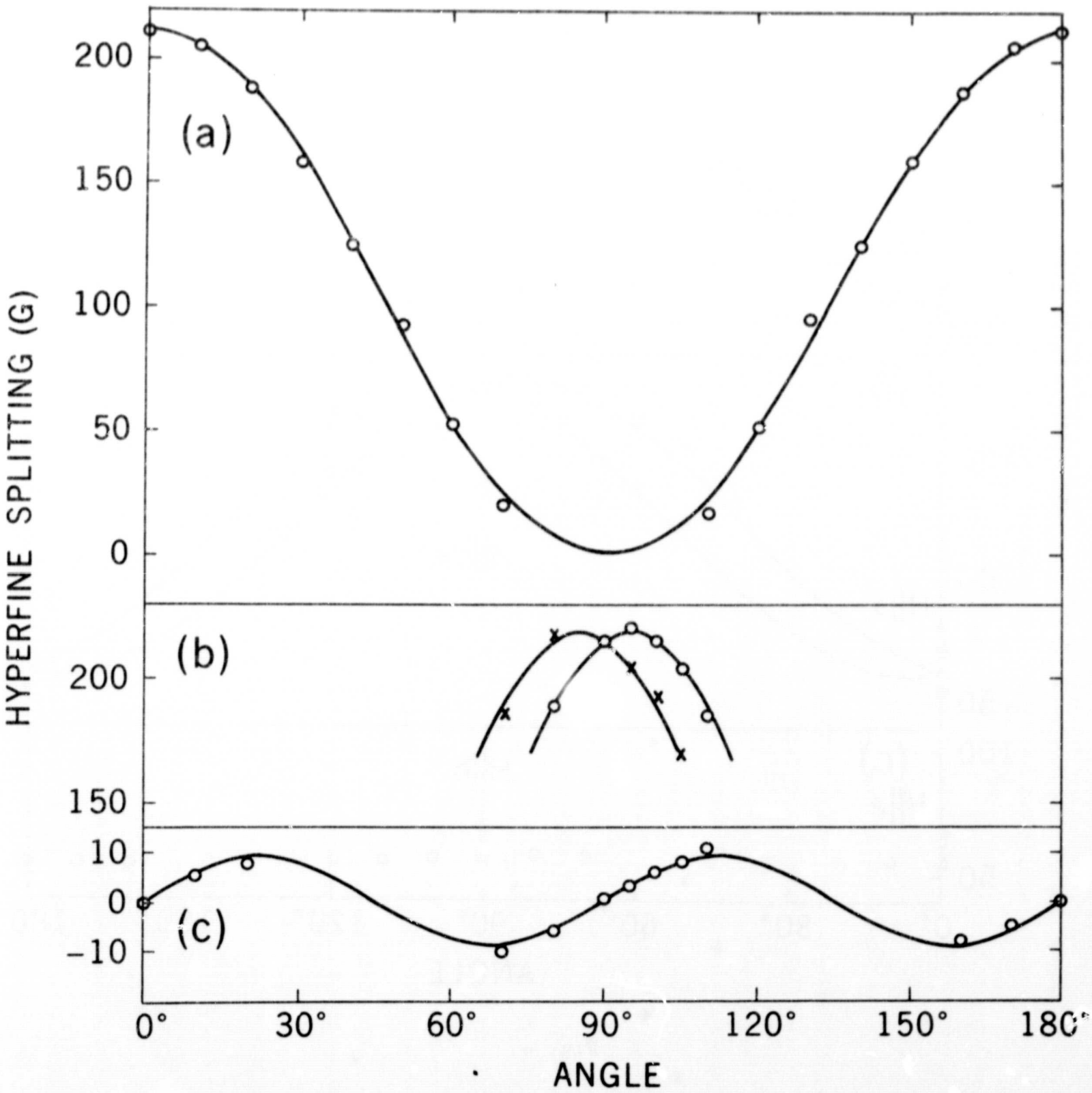
HYPERFINE SPLITTING (G)
200
150
100
50
0
(a)
200
150
(b)
10
0
-10
(c)
0°
30°
60°
90°
120°
150°
180°
ANGLE

Fig. 3

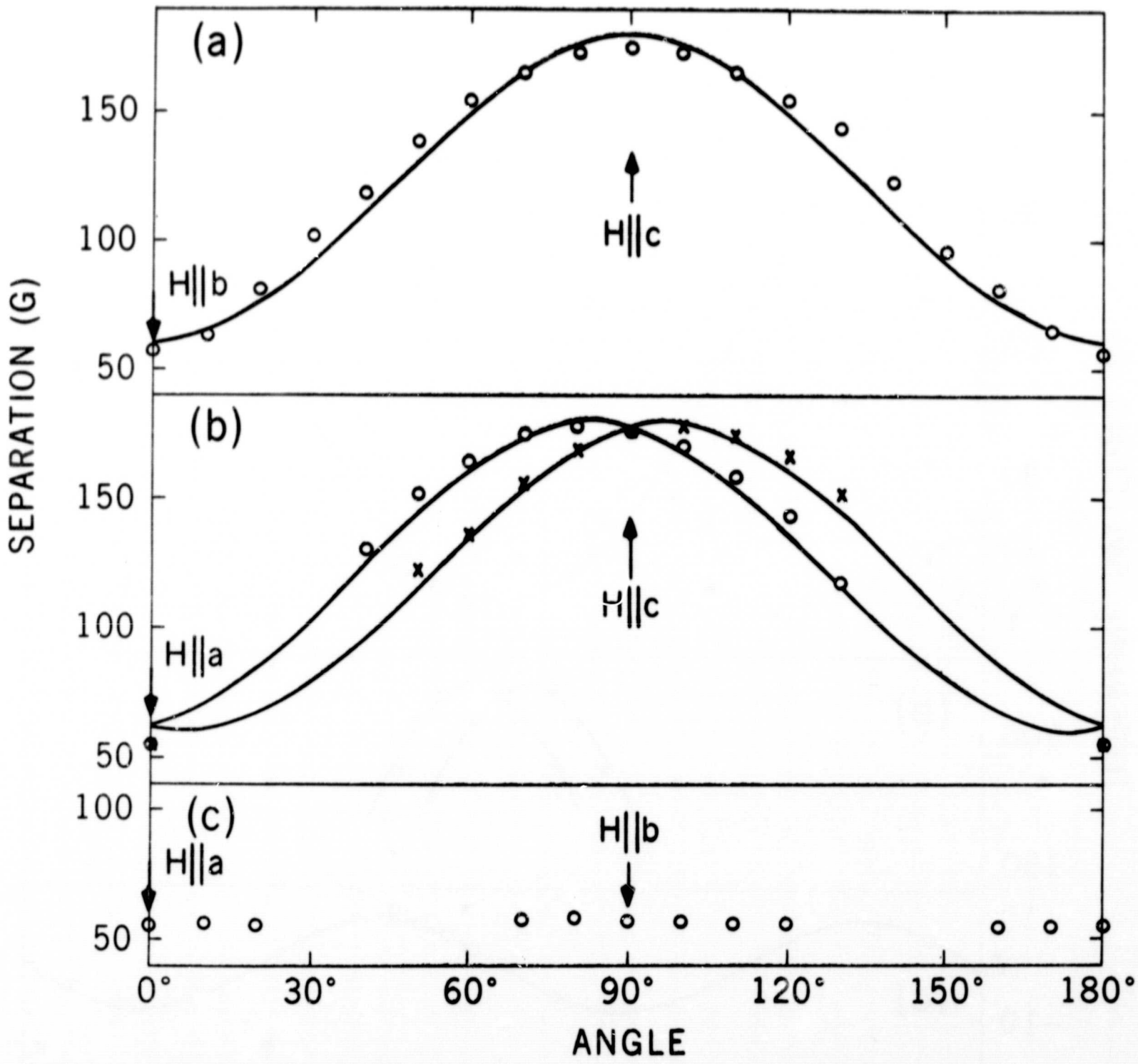
(a)
150
100
50
H||b
H||c
(b)
150
100
50
H||a
H||c
(c)
100
50
H||a
H||b
0°
30°
60°
90°
120°
150°
180°
ANGLE
SEPARATION (G)

Fig. 4

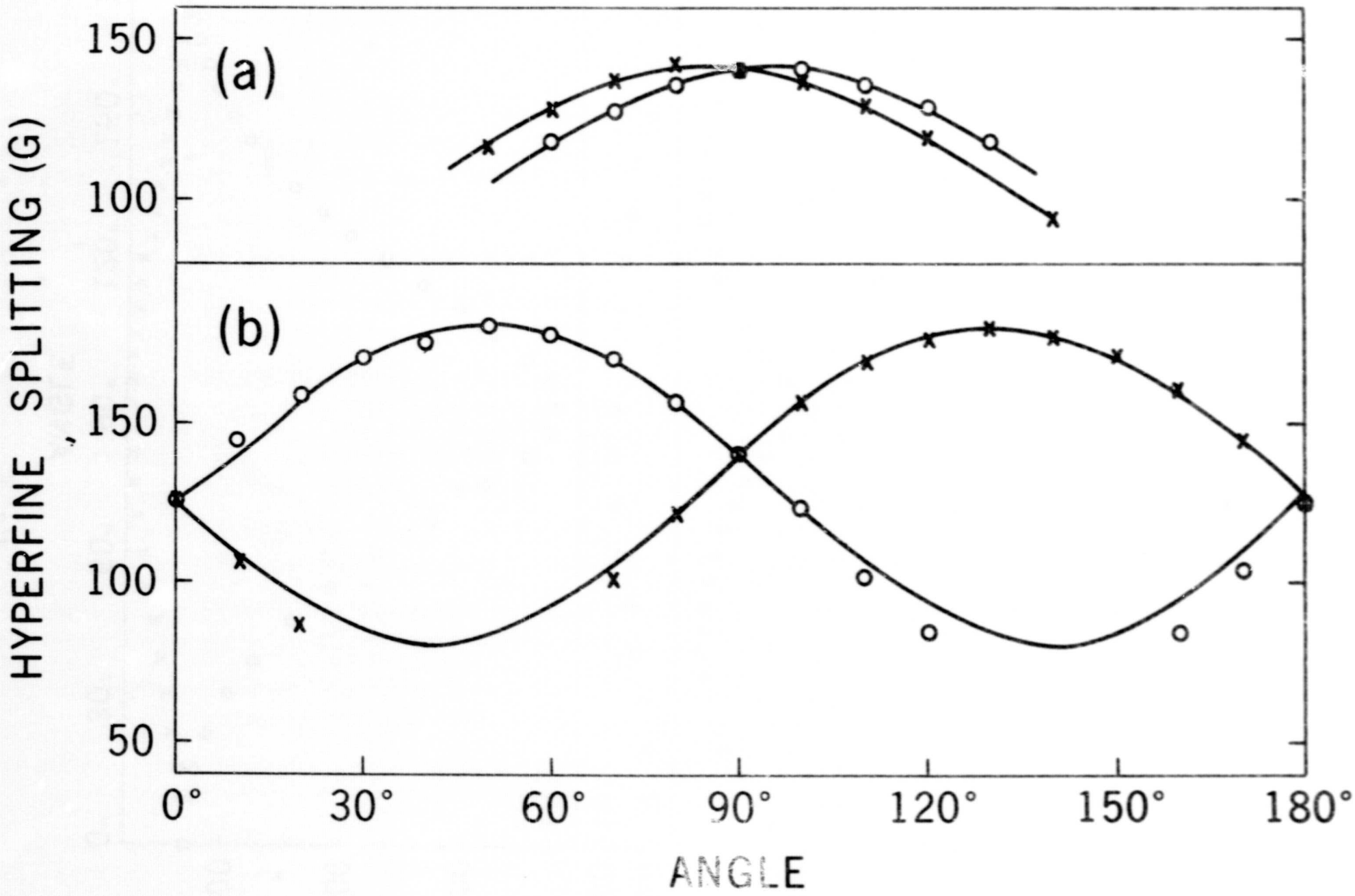
(a)
(b)
150
100
150
100
50
HYPERFINE SPLITTING (G)
0°
30°
60°
90°
120°
150°
180°
ANGLE

Fig. 5

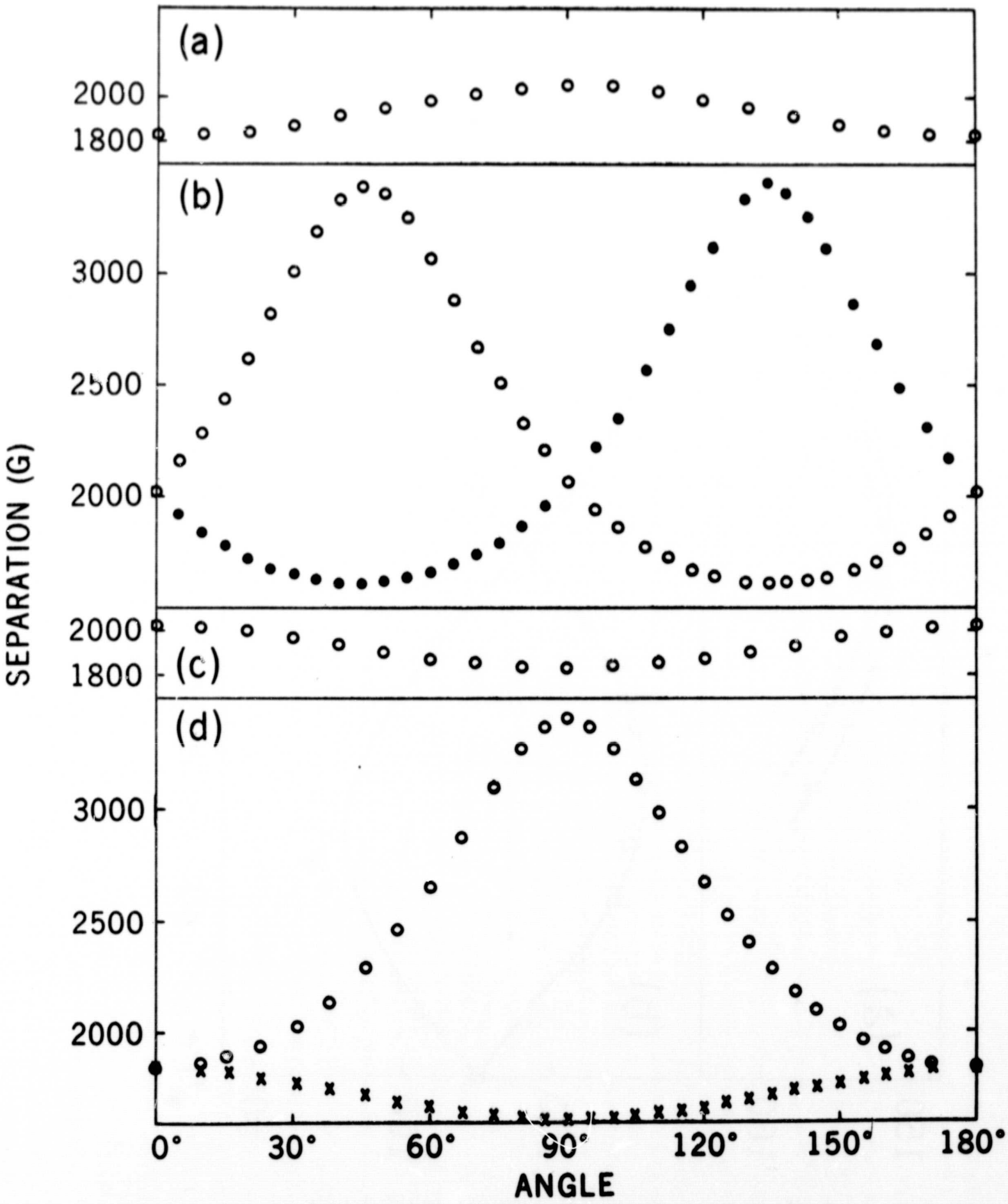
(a)
2000
1800
(b)
3000
2500
2000
(c)
2000
1800
(d)
3000
2500
2000
SEPARATION (G)
0°
30°
60°
90°
120°
150°
180°
ANGLE

Fig. 6

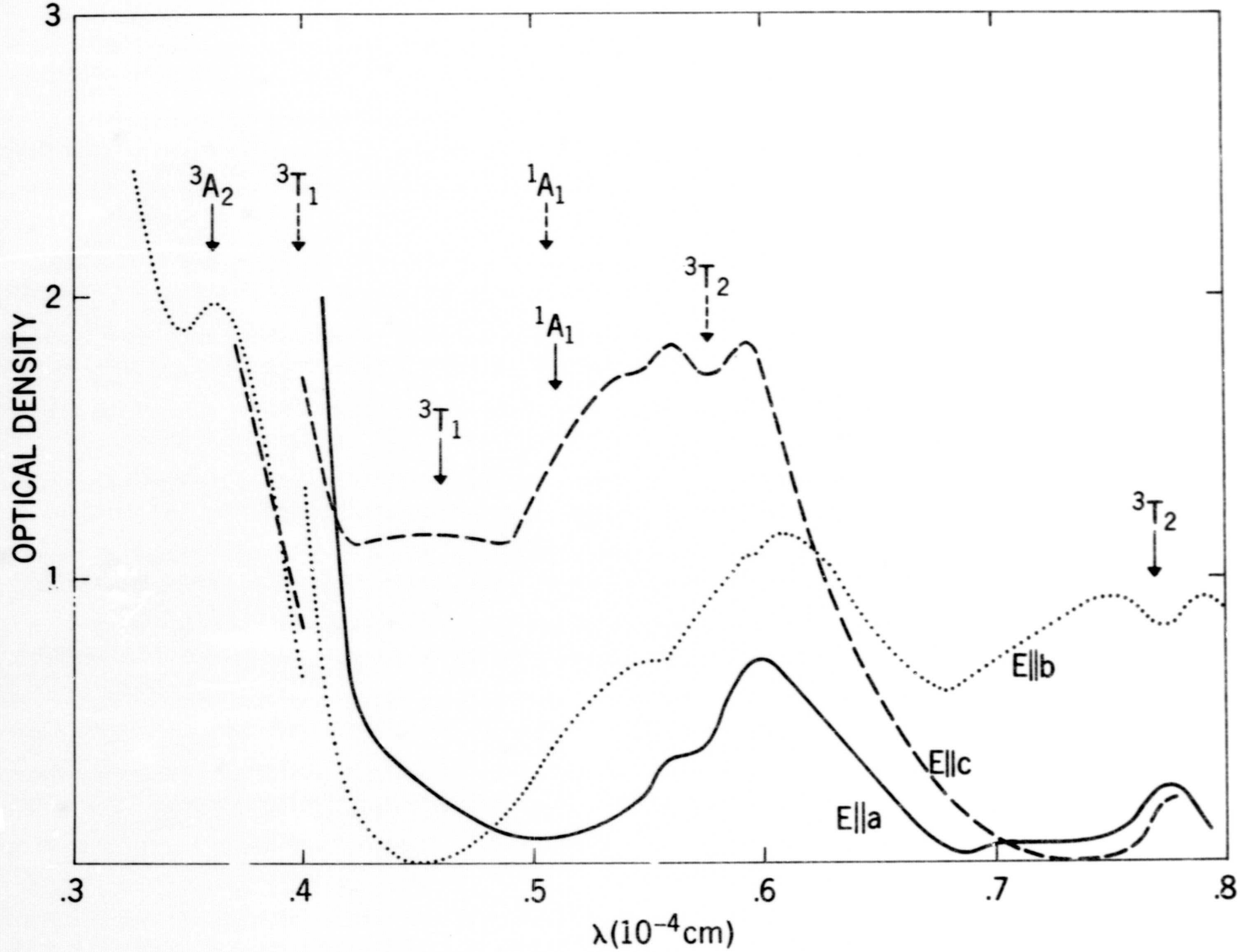
3
2
1
OPTICAL DENSITY
$^3A_2$
$^3T_1$
$^1A_1$
$^3T_2$
$^1A_1$
$^3T_1$
$^3T_2$
E||b
E||c
E||a
.3
.4
.5
.6
.7
.8
λ(i0^{-4}cm)

Fig. 7